RNA Structures

Deutsche Ausgabe: DOI: 10.1002/ange.201509997
Internationale Ausgabe: DOI: 10.1002/anie.201509997

SAM-II Riboswitch Samples at least Two Conformations in Solution in the Absence of Ligand: Implications for Recognition

*Bin Chen[+], Regan LeBlanc[+], and T. Kwaku Dayie**

Abstract: *Conformational equilibria are increasingly recognized as pivotal for biological function. Traditional structural analyses provide a static image of conformers in solution that sometimes present conflicting views. From ^{13}C and ^{1}H chemical exchange saturation transfer experiments, in concert with ligation and selective labeling strategies, we show that in the absence of metabolite, a Mg^{2+} (0–0.5 mM)-bound apo SAM-II riboswitch RNA exists in a minor (≈10%) partially closed state that rapidly exchanges with a predominantly (≈90%) open form with a lifetime of ≈32 ms. The base and sugar (H6,C6, H1′,C1′) chemical shifts of C43 for the dominant conformer are similar to those of a free CMP, but those of the minor apo species are comparable to shifts of CMPs in helical RNA regions. Our results suggest that these transient, low populated states stabilized by Mg^{2+} will likely enhance rapid ligand recognition and, we anticipate, will play potentially ubiquitous roles in RNA signaling.*

While it is widely accepted that biomolecules, such as RNAs, are highly dynamic, it is only recently becoming appreciated that RNAs latently sample multiple conformations in solution as a mechanism for function, especially for the class of RNAs called riboswitches.[1–3] The dramatic increase in the discovery of these riboswitches[1] has been followed by high resolution structures of the bound forms.[4] However, only four riboswitches without their cognate ligands have been structurally characterized.[5] Both high resolution X-ray crystallographic and SAXS analyses indicate that a number of riboswitches (FMN, lysine, preQ1, and SAM-1) adopt the same global conformation in the absence or presence of its cognate ligand.[2,5] For all of these classes of riboswitches that have identical crystal structures for both the unbound and the bound states, how do the cognate ligands that are buried (≈60–100%) within their ligand binding sites enter the binding pocket? For the riboswitches that are unstructured and adopt a structure only in the presence of a ligand, how would the ligand recognize such a disorganized binding pocket? These questions are not purely academic. Considerations of RNA dynamics and flexibility of the ligand binding site are a prerequisite for effective drug design strategies.[6]

To better characterize the functional mechanism of how a riboswitch in the unliganded state eventually finds its globally minimized bound state, we probed a SAM-II riboswitch from the Sargasso Sea metagenome.[7,8] Previous X-ray crystal structural analyses indicated this RNA forms a classic H-type pseudoknot with the SAM metabolite ≈64% buried in a binding pocket located in the center of helix P2b (Figure 1a),[8] and other studies indicated the unliganded SAM-II riboswitch likely exists in multiple conformations.[9–11]

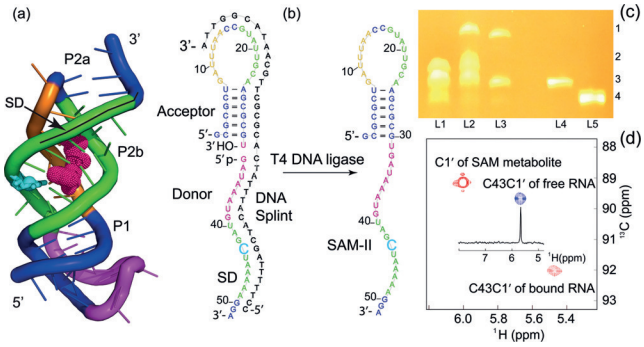

Figure 1. Ligation of SAM-II riboswitch. a) X-ray crystal structure of SAM-II riboswitch (PDB ID: 2qwy).[8] b) Preparation of the segmentally and selectively ^{13}C-labeled, in vitro-transcribed SAM-II RNA. The C43 residue that is selectively ^{13}C-labeled is shown in cyan. c) A 12% denaturing gel showing the ligation results. L1: ligation reaction at 0 h; L2: after 3 h; L3: after DNase digestion; L4: acceptor fragment; L5: donor fragment. Numbers on the right of the panel, 1: ligated product (SAM-II); 2: DNA splint; 3: acceptor fragment; 4: donor fragment. Addition of the DNA splint changed the migration rate of all RNA components in the reaction system. The selectively CTP-labeled donor fragment was almost completely converted to the ligated SAM-II RNA. d) Overlay of 2D $^{1}H/^{13}C$ HSQC spectra of the site-specifically labeled SAM-II riboswitch in the absence (blue) or presence (red) of the metabolite. The intense peak at ≈89 ppm corresponds to a ribose C1′ atom of the SAM metabolite.

SAXS data indicated that the RNA undergoes marked conformational changes and compaction in the presence of Mg^{2+} without the need for the SAM metabolite. However, NMR titration data indicated it is only after the metabolite binds that various secondary and tertiary structural elements form and sequester the SD sequence of the RNA.[11] This conundrum is analagous to the observation that many biological processes sample intermediate states that are only transiently and sparsely populated; therefore, they are

[*] Dr. B. Chen,[+] R. LeBlanc,[+] Prof. T. K. Dayie
Center for Biomolecular Structure and Organization
Department of Chemistry and Biochemistry
University of Maryland
Biomolecular Sciences Building (296)
8314 Paint Branch Dr., College Park, MD 20782 (USA)
E-mail: Dayie@umd.edu
[+] These authors contributed equally to this work.

Supporting information for this article, including the CEST NMR pulse sequence used, is available on the WWW under http://dx.doi.org/10.1002/anie.201509997.

undetectable by traditional NMR and X-ray crystallography techniques.[3,12]

To address this conundrum, we combined ligation, new chemo-enzymatic isotopic labeling strategies, and newly developed NMR dynamics (Chemical Exchange Saturation Transfer, CEST) experiments that probe slow μs–ms motions to detect these otherwise invisible states.[13–16] To the best of our knowledge, this is the first study reporting the measurement of pyrimidine C6 ^{13}C- and ^{1}H-CEST relaxation data in RNA without complications from NOE, thus extending prior purine and ribose ^{13}C-CEST studies on RNA.[16–19]

To probe the formation of the metabolite-binding pocket within helix P2b, a riboswitch variant was constructed using two RNA fragments prepared by in vitro transcription using T7 RNA polymerase (Figure 1 a,b; Supporting Information, Figure S1): an unlabeled 31-nt acceptor fragment was ligated to a 21-nt donor fragment harboring ^{13}C labels at positions 1′ and 6 of residue C43. Mass spectra confirmed the synthesis of the two homogenous RNA fragments (Figure S2). Overall, we obtained a ligated, site-specifically labeled product with typical ligation yields (based on the donor fragment) of ≈80% (Figure 1 c). This selective labeling and ligation approach provided three advantages: unambiguous assignment of C43's C6-H6 and C1′-H1′ resonances without the need of tedious NMR resonance assignment strategies; direct monitoring of the base pair interaction between G22 and C43, as C43 forms the floor of the SAM metabolite binding pocket (Figure 1 a,b, and S1); and straightforward setup and analysis of ^{1}H- and ^{13}C-CEST NMR experiments without complications from strong $^{1}J_{C5C6}$ coupling constant artefacts.[18–20]

A 2D ^{1}H-^{13}C heteronuclear single quantum coherence (HSQC) spectrum obtained for the ligated product in the absence of both Mg^{2+} ion and SAM exhibited a single cross peak that corresponds to ribose C1′ of the residue C43 (Figure 1 d). In agreement with previous studies,[11] the presence of Mg^{2+} ion did not cause any chemical shift change for either C1′ or C6 resonances of C43. Upon addition of SAM metabolite, however, the ribose C1′ carbon resonance shifted considerably from 89.5 ppm to 92.0 ppm, indicating that ligand binding alters the local chemical environment of the C43-C1′ carbon atom. The C43 residue, while flexible in the absence or presence of Mg^{2+} ions (similar longitudinal relaxation time T_1), becomes less flexible (increased T_1) in the presence of both Mg^{2+} ions and metabolite (Figure S3).

Next, application of ^{13}C-CEST to the ligand-free selective and nucleotide-specific C-labeled SAM-II riboswitch, without Mg^{2+}, immediately revealed a conformational state that is opaque to conventional NMR experiments (Figure 2 a). The ^{13}C-CEST profiles of the C43 ribose C1′ atom of the riboswitch, recorded at three different B_1 fields (17.5, 27.9, and 37.8 Hz) with a mixing time (T_{EX}) of 0.3 s at 298 K, indicate an intense dip at 89.5 ppm. This dip matches the C43 labeled peak resonance position in the ^{1}H-^{13}C HSQC spectrum (Figure 1 d) consistent with the ligand-free major state (A) conformation with a characteristic CMP resonance free in solution.[21] Surprisingly, a minor dip corresponding to an invisible second state could be clearly identified in the profiles (Figure 2 a) at a chemical shift of 91.5 ppm ($\Delta\omega$ = 1.61 ppm). This second dip matches the peak position in the ^{1}H-^{13}C HSQC spectrum (Figure 1 d), and the chemical shifts are consistent with a ligand-bound RNA state (B) with characteristic of CMP resonances in helical RNA segments.

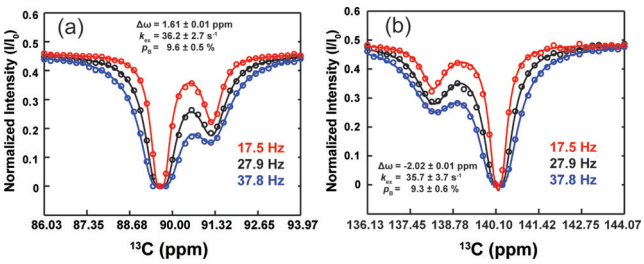

Figure 2. CEST experiments in the absence of Mg^{2+}. a) ^{13}C-CEST profiles of the C43-C1′ atom of the SAM-II riboswitch and b) ^{13}C-CEST profiles of the C43-C6 atom of the SAM-II riboswitch. These were recorded under the same conditions: three different B_1 fields (17.5, 27.9, and 37.8 Hz) in NMR buffer (10 mM sodium phosphate, pH 6.2, 100 mM NaCl, 0.2 mM EDTA, 50 μM DSS, 0.1% sodium azide, 8% D_2O) at a temperature of 298 K with T_{EX} = 0.3 s for C1′ and T_{EX} = 0.2 s for C6.

Thus, a simple visual inspection of the CEST profiles immediately provided structural insights into the nature of the sparsely populated state.

To quantitatively extract the carbon chemical shift ($\Delta\omega$), the exchange rate, and the population of the minor state, a two-state model was fitted to each of the three profiles of the C43 ribose carbon (C1′) and base carbon (C6) separately or together using the Bloch–McConnell 7 × 7 matrix.[22,23] Excellent fits were obtained with the two-state model, as demonstrated by the red, black, and blue curves that match well the experimental data (Figure 2). An exchange rate constant ($k_{ex} = k_{AB} + k_{BA}$) of 36 ± 3 s^{-1} and the population of the invisible state B (P_B)≅9.5 ± 0.5% were obtained from a global fit of both the C1′ and C6 CEST data (Table S1), indicating that the C43 residue as a whole experiences similar chemical exchanges rather than local independent breathing. The lifetime of the state B (τ_B) is 31.0 ± 0.3 ms, which is comparable to recent reports.[10] The extracted chemical shift differences ($\Delta\omega = \omega_A - \omega_B$) of 1.6 and −2.0 ppm between A and B for C43 ribose C1′ and base C6 atoms, respectively, provided important local structural information on the invisible state. Note that because of the selective labeling technologies used here,[19,20] the large $^{1}J_{CC}$ (≈45–60 Hz) couplings are absent with no need to account for these couplings in the data analyses, as was necessary in previous studies that used uniformly labeled samples.[15,16,19,20]

To obtain further insight into the ^{1}H chemical environment of the minor state, the proton chemical shift was determined using a straightforward modification ^{13}C CEST relaxation dispersion experiments with weak off-resonance ^{1}H decoupling (Figure S4).[14,24]

Even though direct ^{1}H CEST experiments are hindered by nuclear Overhauser effects that give rise to artefactual dips in the ^{1}H CEST profile, indirect detection of ^{1}H chemical shifts measured through off-resonance decoupling reveals J_{CH} splitting patterns for the dips of the ^{13}C CEST profile of the ribose C43-C1′ resonance (Figures 2 a, 3 a). The J_{CH} couplings

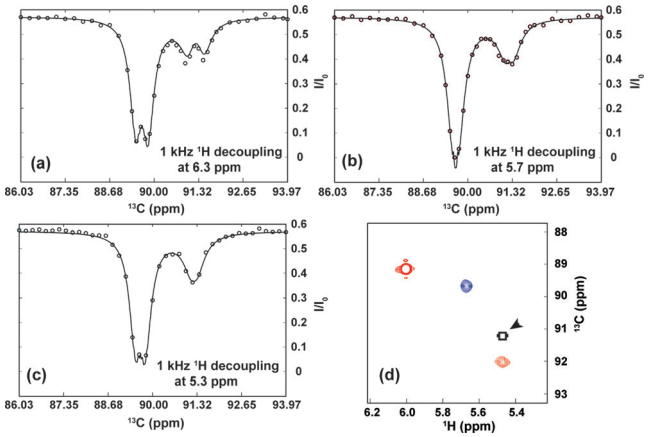

Figure 3. Measurement of ^{1}H chemical shift of the C43-C1′ resonance of the RNA minor state through off-resonance decoupling effects. Three experiments with weak (1000 Hz) proton decoupling were recorded at 6.3 (a), 5.7 (b), and 5.3 (c) ppm, respectively. d) 2D ^{1}H/^{13}C HSQC spectrum of the site-specifically labeled SAM-II riboswitch showing the crosspeaks of C43-C1′ atom in the absence (blue) or presence (red) of the metabolite. An open box symbol indicates the position of the predicted crosspeak of the C43-C1′ and C43-H1′ resonances in the B state, with bars at the left or right of the box indicating the possible range of ^{1}H chemical shifts. These were recorded under the same buffer conditions shown in Figure 2.

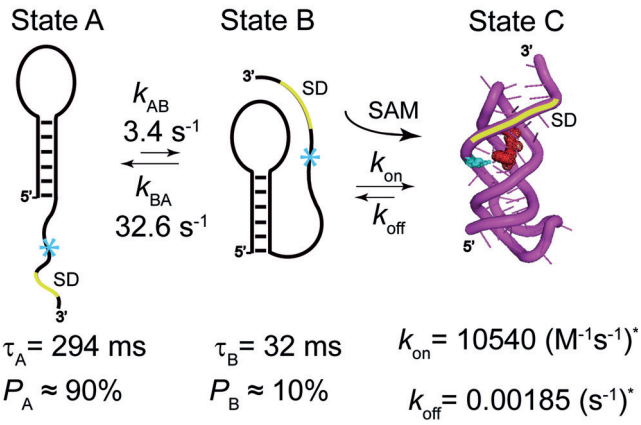

Figure 4. Model illustrating the conformational exchange between states A, B, and C (the X-ray crystal structure of SAM-II riboswitch with a PDB ID: 2qwy).[9] *Rates for k_{on} and k_{off} are the averages of three previously reported pre-steady state fluorescence measurements at 10:1 (ligand:riboswitch) concentrations at 20 °C by Haller and co-workers.[10]

of the major and minor peaks are easily identified in the CEST profile and are dependent on the B_1 field and offset of the ^{1}H decoupler from the major and minor resonances (Figure 3 a–c).

The experimental data was fitted to a two-state exchange Bloch–McConnell 31 × 31 matrix that describes the time-dependent evolution of magnetization during the CEST period.[14,23] Three experiments with weak (1000 Hz) proton decoupling were run at three ^{1}H offsets (6.3, 5.7, and 5.3 ppm). As expected, the splitting of the major peak is completely decoupled when the ^{1}H decoupler is set at 5.7 ppm. The minor state peak is only decoupled at 5.3 ppm and not at 6.3 or 5.7 ppm, indicating that the minor state ^{1}H chemical shift is upfield of the major state ^{1}H chemical shift. An additional CEST experiment with no ^{1}H decoupling during T_{EX} was also recorded, showing complete splitting of both major and minor state peaks which overlap to form three distinct dips in the CEST profile (Figures S5, S6). All four of the experiments were globally fitted to the Bloch–McConnell matrix with errors estimated from 200 Monte-Carlo simulations.

The NMR-invisible proton state is not only shifted into a proton frequency region expected for residues in a Watson–Crick base pair configuration, but also the resulting ^{1}H chemical shift offset matches quite well the chemical shift of ligand bound SAM-II. Thus, the free SAM-2 riboswitch appears to sample a conformation similar to the bound state (Figure 3 d). Collectively, these results suggest the riboswitch adopts at least two conformations: the apo SAM-II exists in a dynamic equilibrium between an open highly populated (A, ≈ 90.5 %) and a partially closed, sparsely populated (B, ≈ 9.5 %) state (Figure 4). This apo state exists with a lifetime of ≈ 31 ms. Addition of Mg^{2+} ions increases the sparsely populated B state (from ≈ 11 % at 0.25 mM to ≈ 22 % at 2 mM) and slightly decreases k_{ex} (28 s^{-1} at 0.25 mM to ≈ 21 s^{-1} at 2 mM), thereby stabilizing the sparsely populated state by 0.6 kcal mol^{-1} (Figure S7 and Table S3). These results also nicely complement earlier MD simulations[9] and smFRET experiments[10] with similar predictions of conformational exchange.

This previous smFRET study probed and observed only the formation of the terminal end (C16-G50) of the pseudoknot in the absence and presence Mg^{2+}.[10] The binding pocket was not monitored directly.[10] However, by focusing on the C43 residue that forms a base triple with G22 and A9 within the SAM ligand binding pocket (Figure 1 a,b and S1), our results indicate that, in the absence of metabolite, increasing Mg^{2+} ion concentrations (0 to 2 mM) increase a minor state (from 9.5 % to 22 %) that resembles the bound state.[10,25] While our observations do not rule out the possibility of alternative folding pathways, these results nonetheless suggest that this bound-like minor state likely follows the initial formation of the terminal end of the pseudoknot observed by Haller and co-workers.[10] SAM-binding, therefore, likely captures this transient, lowly populated state[10] with minimum expenditure of energy.[25]

As anticipated earlier,[2] and from this work and recent findings on various RNAs, the model that begins to emerge for RNA ligand binding is conformational selection coupled with induced fit (Figure 4).[3,25–27] We anticipate that a number of regulatory RNA processes use a similar dynamic mechanism.

Future work will focus on how the minor state population is tunable by temperature, pH, and ion and metabolite concentrations, as seen with many other RNA systems.[3,18,19,26] Of great interest, the SAM-II pseudoknot structure is able to stimulate −1 frameshifting.[27] Our results predict that the population of the Mg^{2+}-induced minor conformation will likely correlate with frameshifting efficiency as a function of the SAM metabolite. These are currently being pursued.

Acknowledgements

The authors acknowledge Andrew P. Longhini and Owen Becette for their help in making selectively isotopically labeled CTP. We thank Qi Zhang for providing Matlab software for fitting CEST data, which was modified for use in this study. We thank the National Institute for General Medical Sciences (P50 GM103297 to T.K.D.), the National Science Foundation (DBI1040158 and CHE1213668 to T.K.D.).

Keywords: conformational dynamics · NMR spectroscopy · riboswitches · RNA · RNA dynamics

How to cite: *Angew. Chem. Int. Ed.* **2016**, *55*, 2724–2727
Angew. Chem. **2016**, *128*, 2774–2777

[1] R. R. Breaker, *Mol. Cell* **2011**, *43*, 867–879.
[2] Q. Vicens, E. Mondragón, R. T. Batey, *Nucleic Acids Res.* **2011**, *39*, 8586–8598.
[3] B. Zhao, Q. Zhang, *Curr. Opin. Struct. Biol.* **2015**, *30*, 134–146.
[4] A. Serganov, E. Nudler, *Cell* **2013**, *152*, 17–24.
[5] J. A. Liberman, J. E. Wedekind, *Wiley Interdiscip. Rev. RNA* **2012**, *3*, 369–384.
[6] R. A. Copeland, *Future Med. Chem.* **2011**, *3*, 1491–1501.
[7] K. A. Corbino, J. E. Barrick, J. Lim, R. Welz, B. J. Tucker, I. Puskarz, M. Mandal, N. D. Rudnick, R. R. Breaker, *Genome Biol.* **2005**, *6*, R70.
[8] S. D. Gilbert, R. P. Rambo, D. Van Tyne, R. T. Batey, *Nat. Struct. Mol. Biol.* **2008**, *15*, 177–182.
[9] J. M. Kelley, D. Hamelberg, *Nucleic Acids Res.* **2010**, *38*, 1392–1400.
[10] A. Haller, U. Rieder, M. Aigner, S. C. Blanchard, R. Micura, *Nat. Chem. Biol.* **2011**, *7*, 393–400.
[11] B. Chen, X. Zuo, Y.-X. Wang, T. K. Dayie, *Nucleic Acids Res.* **2012**, *40*, 3117–3130.
[12] A. Sekhar, L. E. Kay, *Proc. Natl. Acad. Sci. USA* **2013**, *110*, 12867–12874.
[13] N. L. Fawzi, J. Ying, R. Ghirlando, D. A. Torchia, G. M. Clore, *Nature* **2011**, *480*, 268–272.
[14] G. Bouvignies, L. E. Kay, *J. Phys. Chem. B* **2012**, *116*, 14311–14317.
[15] P. Vallurupalli, G. Bouvignies, L. E. Kay, *J. Am. Chem. Soc.* **2012**, *134*, 8148–8161.
[16] B. Zhao, A. L. Hansen, Q. Zhang, *J. Am. Chem. Soc.* **2014**, *136*, 20–23.
[17] B. Zhao, Q. Zhang, *J. Am. Chem. Soc.* **2015**, *137*, 13480–13483.
[18] C. H. Wunderlich, M. A. Juen, R. M. Leblanc, A. P. Longhini, T. K. Dayie, C. Kreutz, *Methods Enzymol.* **2015**, *565*, 461–494.
[19] A. P. Longhini, R. M. Leblanc, O. Becette, C. Salguero, C. H. Wunderlich, B. A. Johnson, V. M. D'Souza, C. Kreutz, T. K. Dayie, *Nucleic Acids Res.* **2015**, DOI: 10.1093/nar/gkv1333.
[20] Y. Zhou, D. Yang, *J. Biomol. NMR* **2015**, *61*, 89–94.
[21] T. K. Dayie, C. S. Thakur, *J. Biomol. NMR* **2010**, *47*, 19–31.
[22] H. M. McConnell, *J. Chem. Phys.* **1958**, *28*, 430.
[23] M. Helgstrand, T. Härd, P. Allard, *J. Biomol. NMR* **2000**, *18*, 49–63.
[24] C. R. R. Grace, R. Riek, *J. Am. Chem. Soc.* **2003**, *125*, 16104–16113.
[25] A. Savinov, C. F. Perez, S. M. Block, *Biochim. Biophys. Acta Gene Regul. Mech.* **2014**, *1839*, 1030–1045.
[26] B. Fürtig, S. Nozinovic, A. Reining, H. Schwalbe, *Curr. Opin. Struct. Biol.* **2015**, *30*, 112–124.
[27] C.-H. Yu, R. C. L. Olsthoorn, *Methods Enzymol.* **2015**, *550*, 385–393.

Received: October 26, 2015
Revised: December 18, 2015
Published online: January 21, 2016

